



Record-breaking flood over the Yangtze River in early summer 2020: role of the north Indian Ocean and north tropical Atlantic SST

Xiaoxue Yin^{1,2} · Lian-Tong Zhou² · Kui Liu^{2,3} · Yongqiu Han² · Zhaoyang Du^{2,4}

Received: 20 August 2021 / Accepted: 19 December 2021 / Published online: 3 October 2022
© The Author(s), under exclusive licence to Springer-Verlag GmbH Austria, part of Springer Nature 2022

Abstract

The Yangtze River valley (YRV) suffered an extreme flood in the early summer (June–July; JJ) 2020, contemporaneous with warm sea surface temperature (SST) over the north Indian Ocean (NIO) and the north tropical Atlantic (NTA) regions. It is suggested that the warm NIO condition played dominant role in the heavy rainfall in China. The present study confirmed the contribution of the NIO warming and examined the underlying processes by conducting statistical analysis. There are two ways by which the NIO SSTAs can influence the flooding in JJ 2020 by reinforcing the anomalous western North Pacific anticyclone (WNPAC). One is through an anomalous Kelvin wave in lower level troposphere that propagates into western Pacific and induces suppressed convection. The other is through a reversed Walker circulation over the Indo-Pacific regions that causes divergent circulation in lower level troposphere around WNP. In addition, we show that the warm NTA SSTAs could also enhance WNPAC and YRV flood through an anomalous zonal vertical circulation, with anomalous ascending motion over the NTA region and anomalous descending motion over tropical central-eastern Pacific. The intensified WNPAC facilitated moisture flux transport to YRV through southwesterly anomalies and resulted in extreme flood over YRV in JJ 2020. This study suggests that the NIO and NTA SSTAs can cause extreme flood event in YRV independent of El Niño–Southern Oscillation (ENSO), which highlights the importance of considering SSTAs over the NIO and NTA regions when predicting extreme climate events in China besides ENSO.

1 Introduction

Located within the East Asian summer monsoon region, summer rainfall accounts for the largest proportion for annual rainfall over eastern China (Wu et al. 2003). The unusual interannual variability of summer rainfall over eastern China is often concurrent with severe droughts and floods, which repeatedly caused immense economic losses and social damage (Chen and Zhai 2013; Huangfu et al. 2018; Jiang et al. 2008; Ohba et al. 2015; Zhou and Chan 2007). For example,

the severe flood that occurred in the summer of 1998 caused 15 million people homeless and huge economic losses (Huang and Zhou 2002; Yuan et al. 2017; Zong and Chen 2000). In early summer (June–July; JJ) of 2020, many regions in eastern China suffered another devastating flood event. This flood hit the mid-to-lower reaches of the Yangtze River valley (YRV) and caused an increase in rainfall amounts up to 63% above the climatological value. Therefore, the variability and prediction of such extreme rainfall events has become a critical and urgent issue in climate research and a great concern to policy-makers (Ding et al. 2020).

Intensive efforts have been made to improve understanding of the physical processes responsible for summer rainfall variability in eastern China. Climatologically, a zonally elongated Meiyu rain-band along YRV in central China is visible in JJ (Zhou and Yu 2005). The interannual variability of Meiyu rainfall over the YRV region is influenced by many factors, including the El Niño–Southern Oscillation (ENSO) event, the Indian Ocean and North Atlantic sea surface temperature anomalies (SSTAs), the western North Pacific (WNP) subtropical high (WNPSH) as well as intra-seasonal variability of the Madden–Julian Oscillation (Chen

✉ Lian-Tong Zhou
zlt@mail.iap.ac.cn

¹ Department of Navigation, China Coast Guard Academy, Ningbo 315801, China
² Center for Monsoon System Research, Institute of Atmospheric Physics, Chinese Academy of Sciences, P.O. Box 2718, Beijing 100190, China
³ College of Geography and Tourism, Hengyang Normal University, Hengyang 421002, Hunan Province, China
⁴ Ningxia Meteorological Observatory, Yinchuan 750002, China

et al. 2020; Gao et al. 2018; Gu et al. 2009; Lau and Weng 2001; Li et al. 2017; Zhang et al. 2019; Zhou and Chan 2007). Variability of these climate modes is considered to affect the occurrence of extreme rainfall events in the YRV.

Tropical SSTAs are recognized as important external forcing that impact the variability of summer rainfall in eastern China. At the interannual timescale, traditional eastern Pacific (EP) ENSO is one of the crucial factors influencing the variability of summer rainfall in eastern China (Huang and Wu 1989; Wu et al. 2003; Zhang et al. 1999, 2019). Previous studies implied a positive correlation between tropical eastern Pacific SSTAs in winter and YRV rainfall anomalies in the following summer. In post-El Niño summer, a large-scale anomalous anticyclone over WNP (WNPAC) is considered as the key bridge for conveying El Niño-related influences to East Asia (Wang and Zhang 2002; Wu et al. 2003). Anomalous WNPAC could enhance summer rainfall in mid-to-lower reaches of YRV by modulating the strength and location of WNPSH and regulating moisture flux transportation to eastern Asia (Chang et al. 2000). Thus, following super El Niño events, extreme Meiyu rainfall floods over YRV often appeared, such as the dramatic floods occurred in 1998 and 2016 (Chen et al. 2018; Gao et al. 2018). In these years, El Niño-related WNPAC intensified the water vapor flux transport from the warm oceans to YRV by southwesterly anomalies, which favored the serious flooding in the YRV (Zhou and Yu 2005).

Maintenance of WNPAC in post-El Niño summer is attributed to remote forcing of warming condition in the Indian Ocean, which contributes to the persistence of WNPAC via a Kelvin wave-Ekman divergence mechanism (Xie et al. 2009) or a zonal overturning vertical circulation over the tropical Indo-Pacific Ocean (Annamalai et al. 2005; He and Wu 2014). Meanwhile, anomalous easterly winds on south side of the anomalous WNPAC maintained the warming condition north Indian Ocean (NIO) by reducing southwest monsoon and surface evaporation (Du et al. 2009). This positive feedback between air-sea interactions in the Indo-WNP region prolongs atmospheric response to El Niño (Kosaka et al. 2013; Xie et al. 2016). In addition, many studies suggested that the anomalous WNPAC is associated with north tropical Atlantic (NTA) SSTAs (Chen et al. 2015; Ham et al. 2013; Hong et al. 2014; Rong et al. 2010). For example, Rong et al. (2010) pointed out that, in post-El Niño summer, positive SSTAs over the NTA region trigger an atmospheric Kelvin wave stretched downstream to equatorial Indo-Pacific region, which causes low-level easterly wind anomalies and strengthens the WNPAC. Hong et al. (2014) found that the impact of tropical Atlantic SST on WNPSH, connected by a zonally overturning vertical circulation anomaly over equatorial central Pacific and tropical Atlantic, was enhanced after the 1980s.

In post-El Niño summer, El Niño can induce SSTAs in the Indian Ocean and tropical Atlantic Ocean through atmospheric

bridges (Klein et al. 1999; Yin and Zhou 2019, 2020). This implies that influences of the Indian Ocean and tropical Atlantic SSTAs on WNPAC may be a linkage for ENSO event. Recent studies implied that WNPAC is associated with SSTAs over the Indian Ocean and tropical Atlantic regions even without ENSO (Kosaka et al. 2013; Chen et al. 2015; Xie et al. 2016). For example, Kosaka et al. (2013) identified a coupled air-sea interaction mode between warming NIO SST and WNPAC when El Niño-related SSTAs are removed. In addition, Chen et al. (2015) indicated an intensified relationship between tropical Atlantic SSTAs and WNPAC with ENSO effect removed. Therefore, it suggests that the NIO and NTA SSTAs may influence the YRV summer rainfall anomalies by modulating WNPAC in years without ENSO.

Recently, the 2020 YRV flooding event has been studied by many researchers on different timescale such as sub-month and sub-seasonal timescales (Ding et al. 2021; Liu et al. 2020; Qiao et al. 2021; Takaya et al. 2020; Zheng and Wang 2021; Zhou et al. 2021). On the sub-month timescales, they found that the North Atlantic Oscillation (NAO) pattern (Liu et al. 2020), mid-latitude teleconnection and the Pacific-Japan (PJ) pattern (Qiao et al. 2021) as well as the quasi-biweekly oscillation (QBWO) (Ding et al. 2021) contributed to the extreme Yangtze flooding. Zheng and Wang (2021) suggested that the enhanced rainfall in June 2020 is regulated by interactions among the Pacific, Atlantic, and Indian Oceans. The NIO SST warming state in summer 2020 is considered as a main contributor to the YRV extreme rainfall in June and July (JJ) (Ding et al. 2021; Zhou et al. 2021). The present study focuses on the processes associated with the extreme flooding event in JJ 2020 and emphasizes the joint influences of the NIO and NTA SSTAs on the YRV rainfall in JJ 2020.

The rest of the paper is organized as follows. Section 2 describes dataset and methods used in the present study. Section 3 presents the features of the record-breaking YRV rainfall in JJ 2020. The influences of the NIO and NTA SSTAs on the anomalous YRV rainfall in JJ 2020 are addressed in Section 4. Section 5 gives the summary and discussion.

2 Data and method

The datasets used in this study are described as follows. The monthly mean rainfall data is from 160 stations of the Chinese Meteorological Data Center in China, which meets the standards of the World Meteorological Organization. The Climate Prediction Center's Merged Analysis of Precipitation (CMAP) is employed with a horizontal resolution of $2.5^\circ \times 2.5^\circ$ and period spanning from 1979-present (Xie and Arkin 1997). The monthly mean SST is from the National Oceanic and Atmospheric Administration (NOAA) Extended Reconstruction version 5 (ERSST.v5b) and has a

resolution of $2.0^{\circ} \times 2.0^{\circ}$ and spans the period from 1854 to present (Huang et al. 2017). The monthly mean horizontal winds, air temperature, specific humidity, sea level pressure, vertical p-velocity, and geopotential height were provided from the National Centers for Environmental Prediction-Department of Energy (NCEP-DOE) Reanalysis 2, with a horizontal resolution of $2.5^{\circ} \times 2.5^{\circ}$ from 1979 to present (Kanamitsu et al. 2002).

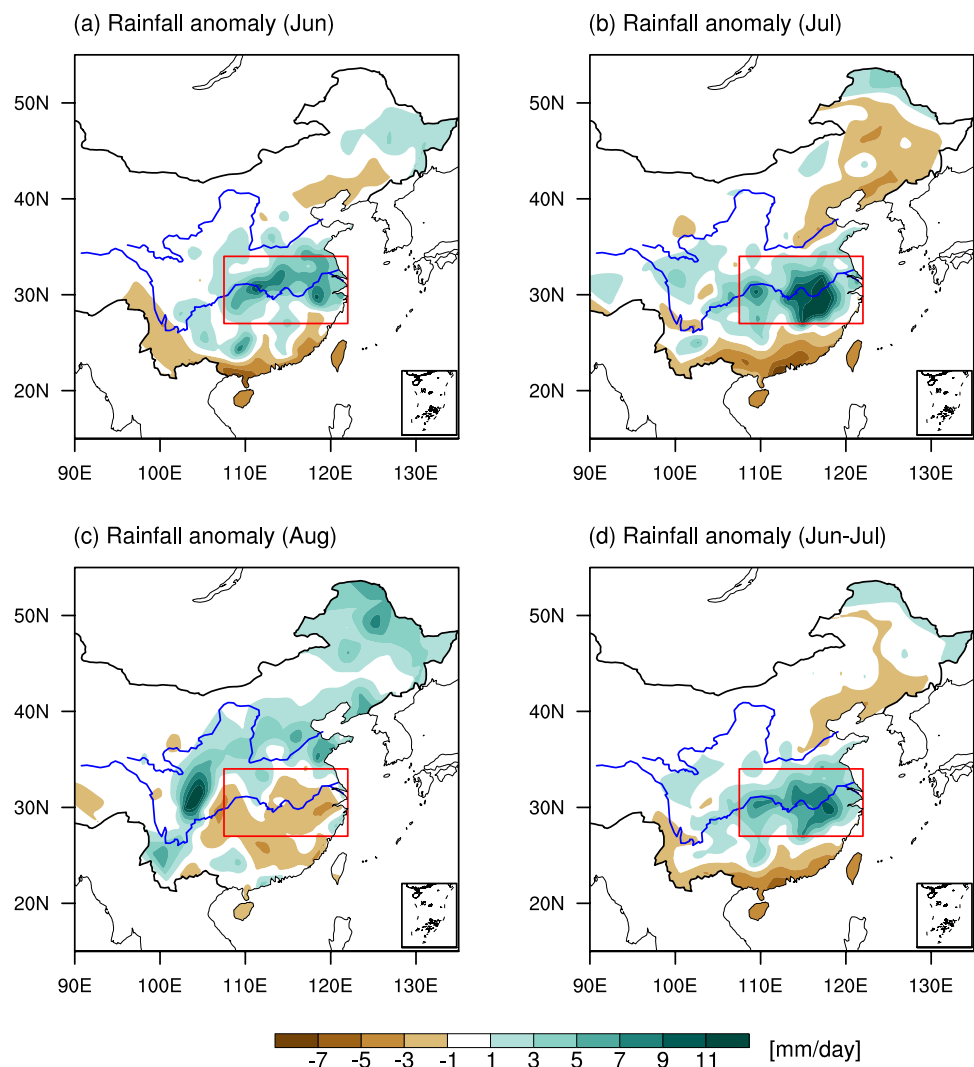
Statistical analysis performed in this study was from 1980 to 2020, in which the monthly anomalies were calculated by removing the 42 years average. The long-term linear trends of all variables were removed to avoid any possible impact of global warming. Linear regression and correlation analyses were applied to examine the relationship between pairs of variables. The statistical significance of these analyses was evaluated using the two-sided Student's *t* test. Partial regression and partial correlation analysis were adopted to measure the relationship between two variables without the effect of other variables. The Niño3.4 index is defined as the averaged

SSTAs in the Niño3.4 region ($5^{\circ} \text{S} - 5^{\circ} \text{N}$, $170 - 120^{\circ} \text{W}$). The NIO SSTAs index is defined as the averaged SSTAs over the region ($0 - 25^{\circ} \text{N}$, $60 - 120^{\circ} \text{E}$). The NTA SSTAs index is defined as the averaged SSTAs over the region ($10 - 22^{\circ} \text{N}$, $90 - 45^{\circ} \text{W}$). The WNPAC is defined as the difference in the 850 hPa westerly wind averaged over a northern region ($20 - 30^{\circ} \text{N}$, $110 - 140^{\circ} \text{E}$) and a southern region ($5 - 15^{\circ} \text{N}$, $100 - 130^{\circ} \text{E}$) (Wang et al. 2001).

3 Features of the record-breaking YRV rainfall

Figure 1 illustrates spatial patterns of rainfall anomaly in summer months of 2020, which are derived from the 160 stations dataset in China. In June and July (Fig. 1a, b), positive rainfall anomalies are mainly located over middle to lower reaches of the YRV. Negative rainfall anomalies are observed over southern China. In August (Fig. 1c), the

Fig. 1 Spatial distribution of rainfall anomalies (mm day^{-1}) over East China in **a** June, **b** July, **c** August, and **d** early summer (June–July mean; JJ) 2020, based on China 160 station data. The red boxes indicate middle to lower reaches of the Yangtze River valley (YRV; $27 - 34^{\circ} \text{N}$, $107.5 - 122^{\circ} \text{E}$)



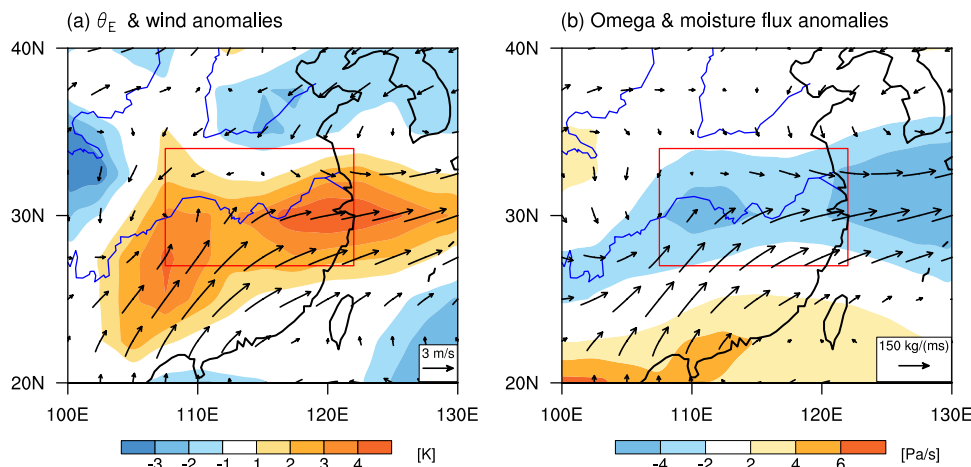
anomalous Meiyu rain-band shifted to northern China and negative rainfall anomalies appeared in the YRV. Therefore, in this study, rainfall anomaly averaged over June and July (hereafter abbreviated as JJ) is chosen to investigate the extreme rainfall in summer 2020 over the YRV. Based on spatial pattern of JJ averaged rainfall anomalies (Fig. 1d), the YRV is defined over the domain [27–34° N, 107.5–122° E]. This definition is similar to the location used in a number of earlier studies (Gong and Ho 2002; Li and Lu 2017; Luo et al. 2013). Thirty-two stations are evenly located across this region (figure is not shown). The rainfall anomaly averaged over these stations is 3.19 mm day⁻¹, 5.22 mm day⁻¹, and -0.82 mm day⁻¹ in June, July, and August, respectively. In JJ, the area-averaged rainfall anomaly in YRV is 4.20 mm day⁻¹, which is approximately 63% more than the average indicated by climatology, resulting in a record-breaking flood in the region in JJ 2020. In the following, the YRV rainfall index (YRVRI) is defined as the JJ rainfall anomalies averaged over these 32 stations.

Strong convective activities and abundant moisture flux transport are two key factors responsible for extreme precipitation events. Figure 2a shows the equivalent potential temperature (θ_e) anomalies and wind anomalies at 850 hPa around the YRV region in JJ 2020. θ_e is determined by both humidity and temperature and has been widely used in Meiyu rainfall research (Chen and Zhai 2015; Zhou et al. 2004). The climatological θ_e decreases with latitude in lower troposphere as warmer and moister air is generally located in the south and the relatively cooler and drier air is occupied in the north (Ding 1992). A positive value of θ_e anomaly indicates a wetter and warmer condition. As shown in Fig. 2a, strong southwesterly wind anomaly is located to the south of the YRV, and weak surface northeasterly wind anomaly is located to the north of the YRV. As a result, positive θ_e anomalies are observed to the south of the YRV, and negative θ_e anomalies are seen to the northern regions. The anomalous θ_e pattern in JJ 2020 intensified the meridional

gradient of the θ_e in the YRV, which is helpful for northward advection of the θ_e and generation of convective instability over the YRV (Ninomiya and Shibagaki 2007). The major region covered with intensified θ_e gradient corresponds well with that overlapped with enhanced rainfall in Fig. 1d. Figure 2b shows the vertical motion anomaly at 500 hPa as well as the column-integrated moisture flux anomaly in JJ 2020. Strong upward motion anomaly is seen along the YRV. Abundant moisture flux was transported to the YRV by the anomalous southwesterly wind from oceans in the subtropics and tropics. These water vapor flux anomalies converge over the YRV and favor the heavy rainfall there. Thus, the strong upward movement and the abundant moisture flux transportation contributed to the extreme flood event over the YRV in JJ 2020.

To obtain a comprehensive picture of the flood situation, Fig. 3 further illustrates the spatial pattern of large scale summer rainfall and atmospheric circulation anomalies in JJ 2020. The remarkable positive rainfall anomalies in YRV are also detected in the GPCP (Fig. 3a) and CMAP (figure is not shown) dataset in JJ 2020. Besides, negative rainfall anomalies occupy the South China Sea (SCS) and WNP regions. The dipole rainfall anomaly pattern resembles the Pacific-Japan (PJ) teleconnection pattern (Huang and Li 1988; Nitta 1987), which provides a crucial connection in climate variability between tropics and midlatitude regions. In its positive phase, the PJ pattern brings a wetter summer to central China, Korea, and Japan (Huang and Sun 1992; Wakabayashi and Kawamura 2004), such as the summers of 1993 and 1998. An anticyclonic wind anomaly is observed over the WNP region. The anomalous southwesterly wind along the northwestern flank of the anomalous anticyclone favorable substantial water vapor flux transport to the YRV from the SCS and WNP regions. Corresponding with the WNPAC, the WNPSH was enhanced and extended more southwestward compared to the climatological result (Fig. 3b). As shown by previous studies (Chen et al. 2019;

Fig. 2 Enhanced rainfall conditions averaged during JJ 2020. **a** 850 hPa equivalent potential temperature (θ_e) anomaly (shadings; K) and wind anomaly (vectors; m s⁻¹). **b** 500 hPa vertical motion anomaly (shadings; 10⁻² Pa s⁻¹) and column integrated moisture flux anomaly (vectors, surface to 300 hPa; kg m⁻¹ s⁻¹). The red box indicates the YRV



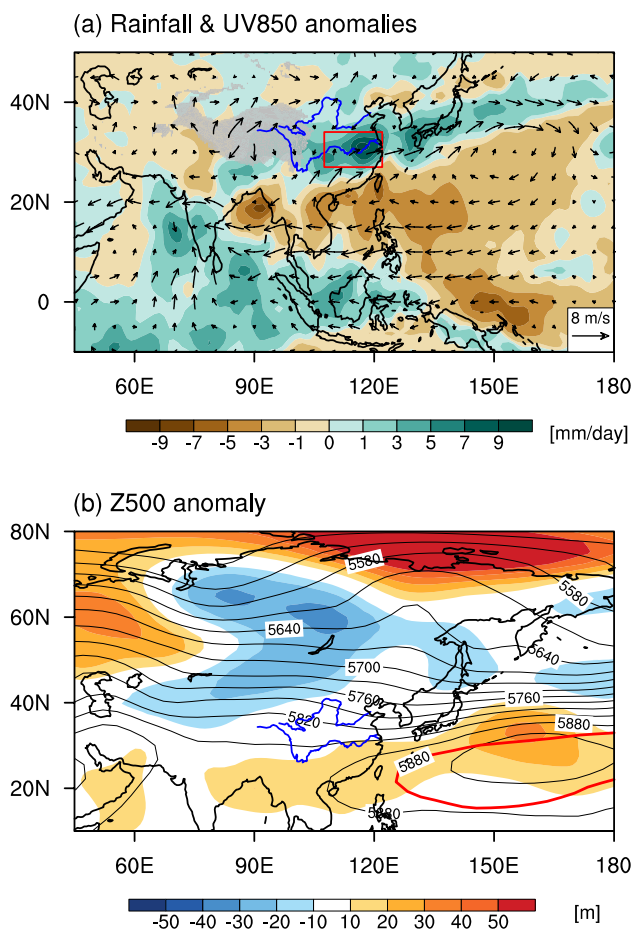


Fig. 3 **a** Rainfall anomaly (shadings; mm day^{-1}) and 850 hPa wind anomaly (vectors; m s^{-1}), **b** 500 hPa geopotential height (contours; gpm) and its anomalies (shadings) averaged during JJ 2020. The red box in **a** indicates the YRV. The red contour in **b** indicates the 5880 gpm line averaged during 1980–2020

Gao et al. 2018; Guo et al. 2002), a southwestward shifted WNPSH is favor for positive rainfall anomalies in the YRV region by modulating moisture flux transport. In addition, atmospheric circulation was strengthened in middle and high latitudes over the Eurasian continent, with a stronger ridge around the Ural Mountain and a deeper trough over the Lake Baikal. According to the Omega equation (Holton 2004), anomalous trough induces ascent motion anomalies in areas ahead of the trough, which favors positive rainfall anomalies in the YRV region.

In this section, we have used monthly data to identify the features of the record-breaking YRV rainfall and large scale atmospheric circulation anomalies in JJ 2020. The analysis shows that anomalous strong WNPAC is the key system that contributes to the extreme flood in the YRV by transporting abundant moisture fluxes. In the following, we will explore the major factors responsible for the anomalous WNPAC from the aspect of external forcing.

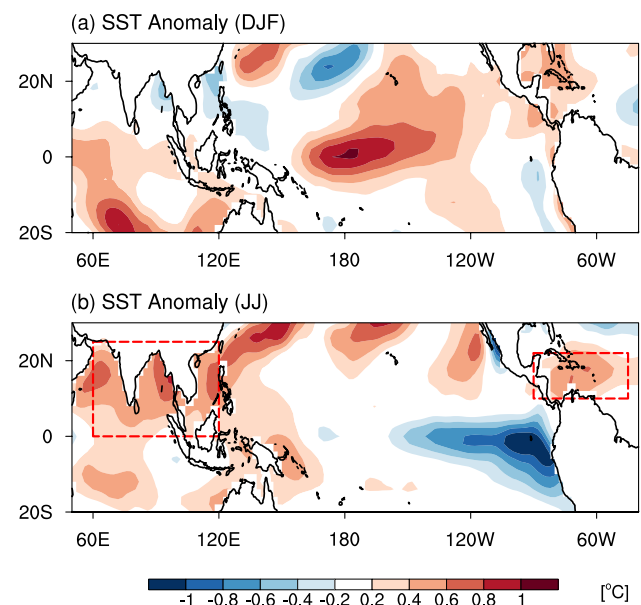


Fig. 4 SST anomalies ($^{\circ}\text{C}$) averaged during **a** December–January–February (DJF) and **b** JJ 2020. In **b**, the red boxes indicate the NIO and SCS region ($0\text{--}25^{\circ}\text{N}$, $60\text{--}120^{\circ}\text{E}$) and the NTA region ($10\text{--}22^{\circ}\text{N}$, $90\text{--}45^{\circ}\text{W}$), respectively

4 Role of the NIO and NTA SSTAs

The above prominent atmospheric conditions in JJ 2020, which were featured by a southwestward shifted WNPSH and a strong WNPAC, are quite similar with the regression maps with respect to the Niño3.4 index in preceding winter obtained by Wu et al. (2003). In fact, the extreme summer rainfall events, such as 1998 and 2016, are closely connected to strong El Niño events in preceding winter (Chen et al. 2018; Gao et al. 2018), with a standardized Niño3.4 index of 2.04 and 2.32 for 1998 and 2016, respectively. In strong post-El Niño summers, warm conditions in the Indian Ocean and SCS were often generated, which could anchor and enhance the anomalous WNAPC, known as the Indo-western Pacific Ocean Capacitor (IPOC) mode (Xie et al. 2016). In preceding winter of 2020, no significant SSTAs are visible in the eastern equatorial Pacific (Fig. 4a). Positive SSTAs are located over the central equatorial Pacific. This SSTAs pattern suggests that a weak CP El Niño event (Ashok et al. 2007) occurred in preceding winter of 2020. In the simultaneous JJ (Fig. 4b), negative SSTAs are located in the eastern equatorial Pacific, which indicates a transition to La Niña. In addition, positive SSTAs are observed over the NIO and NTA regions in JJ 2020. The following analysis will be focused on the possible influences of the warming SSTAs over the NIO and NTA regions on the anomalous WNPAC and rainfall over YRV in JJ 2020.

Figure 5a shows the evolution of three months mean SSTAs indices and the WNPAC index from preceding

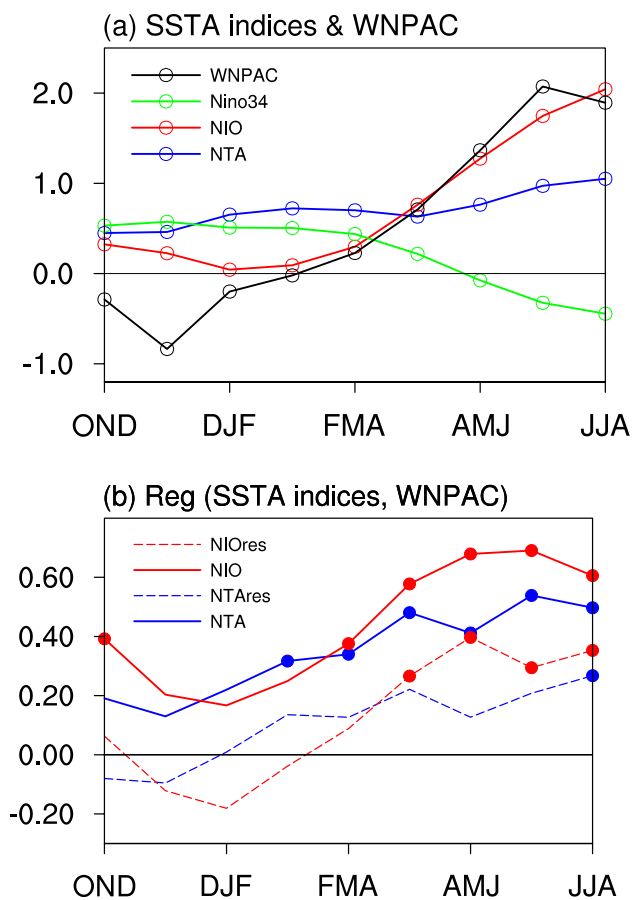


Fig. 5 **a** Evolution of the normalized Niño 3.4 SSTAs index (5° S– 5° N, 170° – 120° W; green curve), NIO SSTAs index (red curve), NTA SSTAs index (blue curve), and the WNPAC index (black curve) smoothed by using a 3-month running from October–November–December 2019 to June–July–August 2020. **b** Lead-lag regression coefficients of WNPAC with respect onto the NIO (red solid line) and NTA (blue solid line) SSTAs indices for JJ during 1980–2020, respectively, and lead-lag partial regression coefficients of WNPAC with respect onto the NIO (red dashed line) and NTA (blue dashed line) SSTAs indices for JJ during 1980–2020, excluding the Niño3.4 effect in preceding winter. The filled circles in **b** denote that the regression coefficients exceeded the 90% confidence levels based on the Student's *t* test

October–November–December (OND) in 2019 to June–July–August (JJA) in 2020. The result shows that the standardized Niño3.4 index is rather weak from preceding winter to following summer, with an amplitude below 0.5. Positive SSTAs in the NTA region appeared since preceding winter and enhanced slightly in summer. The NIO SSTAs exhibited a warm condition from spring and persisted and enhanced sharply in summer. It is also notable that the evolution of the standardized WNPAC index corresponds well with that of the NIO SSTAs index since early spring. Figure 5b further displays the lead-lag regression coefficients of WNPAC index upon the NIO and NTA SSTAs indices in JJ during 1980–2020 from preceding OND in 2019 to JJA

in 2020. Positive correlations are obtained for both the NIO and NTA SSTAs indices connected with the WNPAC index. The remarkably positive NIO-related WNPAC value persists from February–March–April (FMA) to JJA. Lead-lag partial regression analysis onto the NIO index, which excludes the effect of Niño3.4 SSTAs, captures similar features except for a weaker amplitude. This result is consistent with the findings in previous studies (Kosaka et al. 2013; Xie et al. 2016) which suggested that the anomalous anticyclonic system over the WNP is coupled with the positive SSTAs over the NIO and SCS regions even without the effect of ENSO. The significant WNPAC related to the NTA index persists from January–February–March to JJA. Without the effect of ENSO, the partial regression result onto the NTA index is weak and only significant in summer time. This partial regression corresponds with the results obtained by previous studies which found a significant connection between the NTA SSTAs and the anomalous anticyclone over the WNP when the Niño3.4-related SSTAs in preceding winter were excluded (Ham et al. 2013; Hong et al. 2014). Thus, statistically speaking, the close connections between the above two SSTAs indices and the WNPAC index during 1980–2020 imply important impacts from the NIO and NTA SSTAs on the anomalous WNPAC in JJ 2020.

The statistical correlations between the NIO and NTA SSTAs and the YRV summer rainfall in 2020 are verified in Fig. 6 and Fig. 7. Figure 6a shows time series of the normalized YRVRI and the two SSTAs indices. The standardized NIO index reached its peak with a value of 1.87 standardized deviation (SD) in JJ 2020 for the period since 1980. The value of the standardized NTA index is 1.33 SD in JJ 2020. The correlation coefficient between the YRVRI and the NIO (NTA) SSTAs index is 0.54 (0.26), which is significant at the 99% (90%) confident level. This result suggests a positive correlation between the NIO and NTA SSTAs with the YRV summer rainfall during 1980–2020. This is further confirmed by the SSTAs pattern that regressed onto the YRVRI (Fig. 6b). In general, the interannual variability of summer rainfall in the YRV is significantly correlated with SSTAs in the NIO region, NTA region and the tropical eastern Pacific.

Figure 7 shows the reconstructed rainfall anomaly pattern in JJ 2020 using the NIO and NTA SSTAs indices, based on the linear regression approach. There is an obvious meridional dipole rainfall pattern anomaly over East Asia and WNP for both the two SSTAs indices, which is consistent with the anomalous JJ rainfall pattern occurred in 2020 (Fig. 3a). Positive rainfall anomalies are located from middle to lower reaches of the YRV region to most parts of Japan; negative rainfall anomalies are situated over a large area around the Philippines Seas. An anticyclonic wind anomaly is observed over the WNP for both SSTAs indices. The southwesterly wind anomalies lead to the positive rainfall

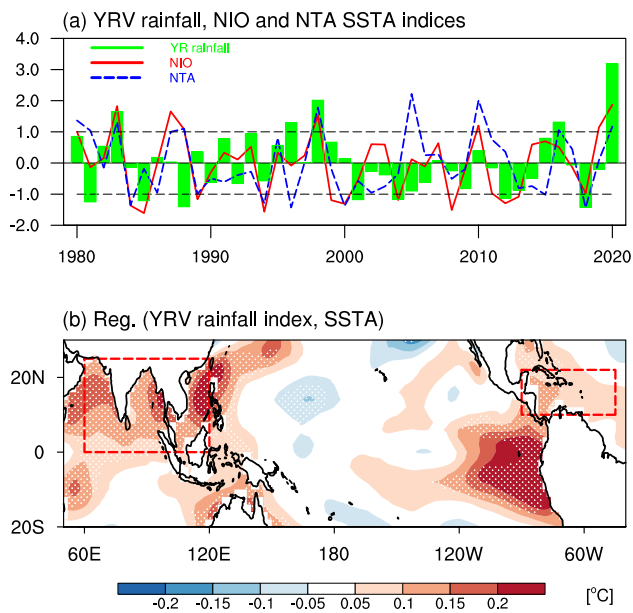


Fig. 6 **a** Time series of the normalized YRV rainfall index (YRVRI; green bar), NIO SSTAs index (red curve) and NTA SSTAs index (blue dashed curve) averaged during JJ 2020. Black dashed lines indicate the one standardized deviation. **b** JJ averaged SST anomalies (shadings; °C) regressed onto the YRVRI during 1980–2020. Dotted regions indicate the 90% confidence level based on Student's *t* test, and red box indicates the NIO and NTA regions, respectively

anomalies in the YRV region by transporting abundant water vapor flux from the WNP and SCS regions. The amplitude and the range of the reconstructed rainfall anomaly related to the NIO index in the YRV region are larger than that related to the NTA index, which indicates a larger contribution to the YRV JJ rainfall anomalies from the NIO SSTAs than that from the NTA SSTAs. Therefore, both the NIO and NTA SSTAs jointly resulted in the record-breaking YRV flood in 2020 summer with the NIO SSTAs dominated.

The above results show a link between the NIO and NTA SSTAs with the anomalous WNPAC as well as the rainfall anomalies over the YRV in JJ 2020 using statistical analysis. In the following analysis, we will explain the possible physical processes through which the NIO and NTA SSTAs can force the anomalous WNPAC, which then results in the rainfall anomalies in the YRV.

4.1 Role of the NIO SSTAs

Based on the above analysis, the warming condition over the NIO is likely to be one of the key factors that induce the extreme rainfall over the YRV in JJ 2020 by modulating the WNPAC. The role of the NIO SSTAs in the climate variability over the WNP has been discussed in many previous studies (Li et al. 2008; Xie et al. 2016; Yang et al. 2007). Two primary mechanisms have been implied to explain the

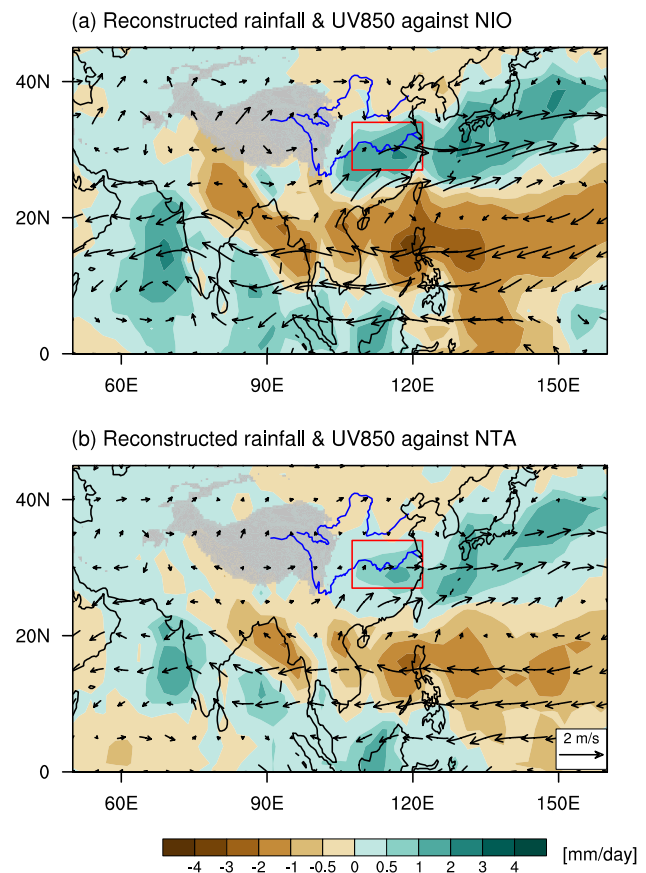
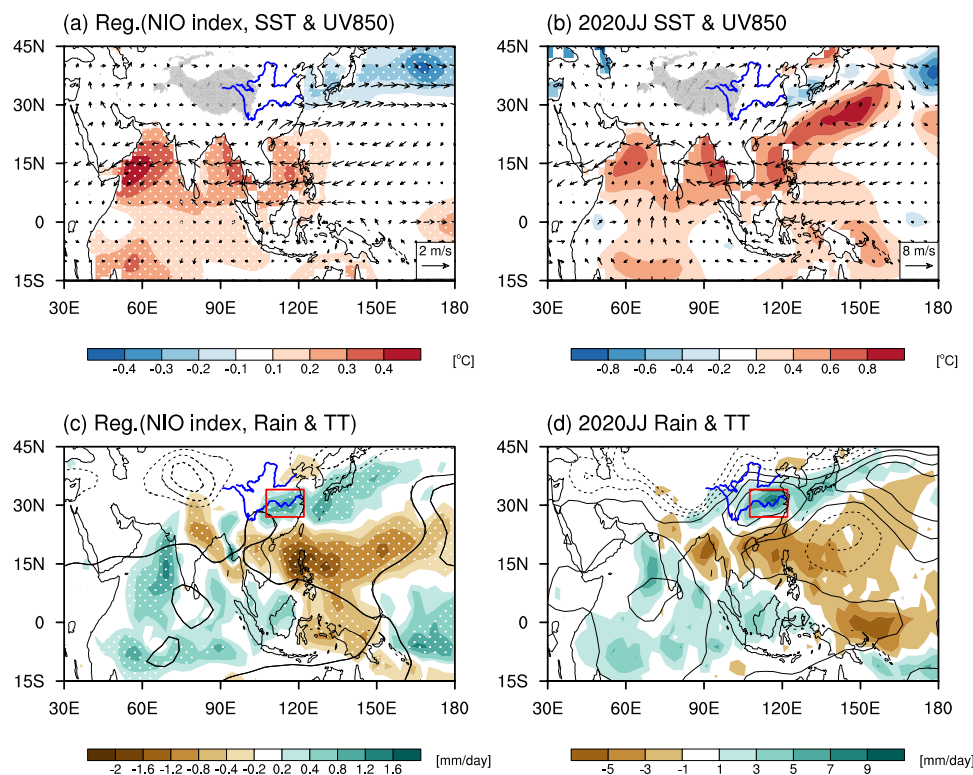


Fig. 7 Reconstructed rainfall anomaly (shadings; mm day^{-1}) and 850 hPa wind anomaly (vectors; m s^{-1}) averaged in JJ 2020 against **a** the NIO SSTAs index and **b** the NTA SSTAs index. Red boxes indicate the YRV region

physical processes connecting the positive SSTAs over the NIO and the anomalous WNPAC, which includes the Kelvin wave induced Ekman divergence (WIED) mechanism (Xie et al. 2009) and the anomalous zonal overturning circulation between the NIO and SCS-Philippine Sea (Annamalai et al. 2005; He and Wu 2014). The following analysis implied that both the above two processes forced by the warming NIO SSTAs were visible in JJ 2020, which made it possible for the enlargement and maintenance of the anomalous WNPAC.

To further understand the forcing impacts from the NIO SSTAs, regressed maps of anomalous SST, 850-hPa winds, rainfall and tropospheric temperature with respect onto the NIO SSTAs index during 1980–2020 as well as the anomalies in JJ 2020 are shown in Fig. 8. There are positive SSTAs (Fig. 8a) and rainfall anomalies (Fig. 8c) located over the NIO region, which suggest that a moist-adiabatic adjustment mechanism for the SSTAs forcing of tropospheric temperature (Emanuel et al. 1997). The anomalous tropospheric temperature displays a Matsuno-Gill pattern, which is consistent with the localized heating in the NIO region and

Fig. 8 Regression pattern of **a** SST (shadings; °C) and 850 hPa wind (vectors; m s^{-1}), **c** rainfall (shadings; mm day^{-1}) and tropospheric (850–250 hPa mean) temperature (contours for $-0.4, -0.3, -0.2, 0.2, 0.3, 0.4$; K) with respect to the normalized NIO SSTAs averaged during JJ for the 1980–2020 period. **(b, d)** Same as **(a, c)**, but for anomalies in JJ 2020 (contours are $-0.75, -0.45, -0.15, 0.15, 0.45, 0.75$; K). Dots in **(a, c)** denote where the regression coefficients exceed the 90% confidence level based on Student's t test. Red boxes in **(b, d)** indicate the YRV region

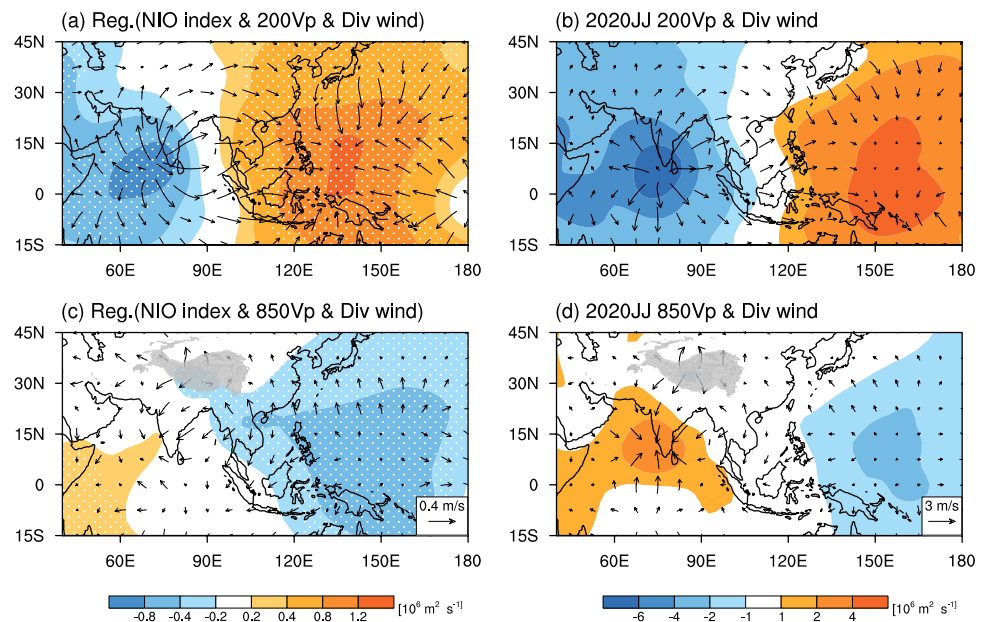


featured by a baroclinic Kelvin wave-like wedge penetrating into the western Pacific along the equator (Fig. 8c). This tropospheric warming triggers the suppression of convection over the subtropical WNP by inducing surface northeasterly wind anomalies and surface Ekman divergence to the north of the equator (Xie et al. 2009). As a result, an anomalous anticyclone develops over the WNP (Fig. 8a), which is accompanied by decreased rainfall anomalies (Fig. 8c). An anomalous cyclone is centered over the East China Sea and Japan (Fig. 8a). This anomalous cyclone is likely forced by the anomalous upper-tropospheric convergence related to the suppressed convection over the subtropical WNP through a PJ-like teleconnection (Nitta 1987). Strong southwesterly wind anomalies on the western flank of the anomalous anticyclone transport abundant moisture flux from the SCS region and increase summer rainfall over eastern China and Japan. In addition, easterly wind anomalies on the southern flank of the WNPAC weaken the prevailing southwesterly monsoon and maintain the NIO warming by reducing surface evaporation (Du et al. 2009). Therefore, the positive atmosphere–ocean feedback over the NIO–WNP region, in which the warming SSTAs over the NIO causes the WNPAC via the warm tropospheric Kelvin wave and the anomalous easterly winds on the southern flank of the WNPAC enhance the NIO warming, results in the formation and maintenance of the strong WNPAC and the extreme flood over the YRV in JJ 2020. The regressed results are similar with that in JJ 2020 (Fig. 8b, d). As shown in Fig. 8b, significant positive

SSTAs dominate the NIO region. A remarkable lower-level anticyclone occupies the SCS and WNP regions. In Fig. 8d, a warm tropospheric Kelvin wave wedge penetrates into the tropical western Pacific; positive and negative rainfall anomalies are located over the Meiyu band and the WNP region, respectively. Therefore, it is convinced that the NIO warming can induce the anomalous WNPAC and positive rainfall anomalies over the YRV in JJ 2020.

In addition, an anomalous reversed Walker circulation over the tropical Indo-Pacific Ocean is observed in the field regressed by the NIO index (Fig. 9a, c) and in JJ 2020 (Fig. 9b, d). The NIO region is overlaid by an anomalous upper-level divergence (Fig. 9a, b) and an anomalous lower-level convergence (Fig. 9c, d), which suggests an enhanced anomalous ascending motion there. According to Lindzen and Nigam (1987), this circulation anomaly represents an atmospheric response to the NIO warming which could induce enhanced convective heating. At upper level, anomalous divergent winds flow from the NIO to tropical western Pacific. Opposite potential velocity anomalies and corresponding divergent wind anomalies are seen over the tropical western Pacific, featuring by an anomalous upper-level convergence and an anomalous lower-level divergence. An anomalous zonal overturning circulation thus forms over the Indo-Pacific region. Descending branch of the anomalous overturning circulation in the western Pacific contributes to the development and enhancement of the WNPAC. Therefore, in JJ 2020, the NIO warming could also contribute to

Fig. 9 Regression pattern of velocity potential (shadings; $10^6 \text{ m}^2 \text{ s}^{-1}$) and the corresponding divergent winds (vectors; m s^{-1}) at **a** 200 hPa and **c** 850 hPa with respect to the normalized NIO SSTAs index averaged during JJ for the 1980–2020 period. **(b, d)** Same as **(a, c)**, but for anomalies in JJ 2020



the development of the WNPAC by inducing a direct and thermally driven divergent circulation over the Indo-Pacific region. This result is consistent with previous findings which indicated that the positive SSTAs over the NIO could induce an anomalous anticyclone over the WNP by an anomalous zonal overturning circulation between the NIO and SCS-Philippine Sea regions (Annamalai et al. 2005; He and Wu 2014).

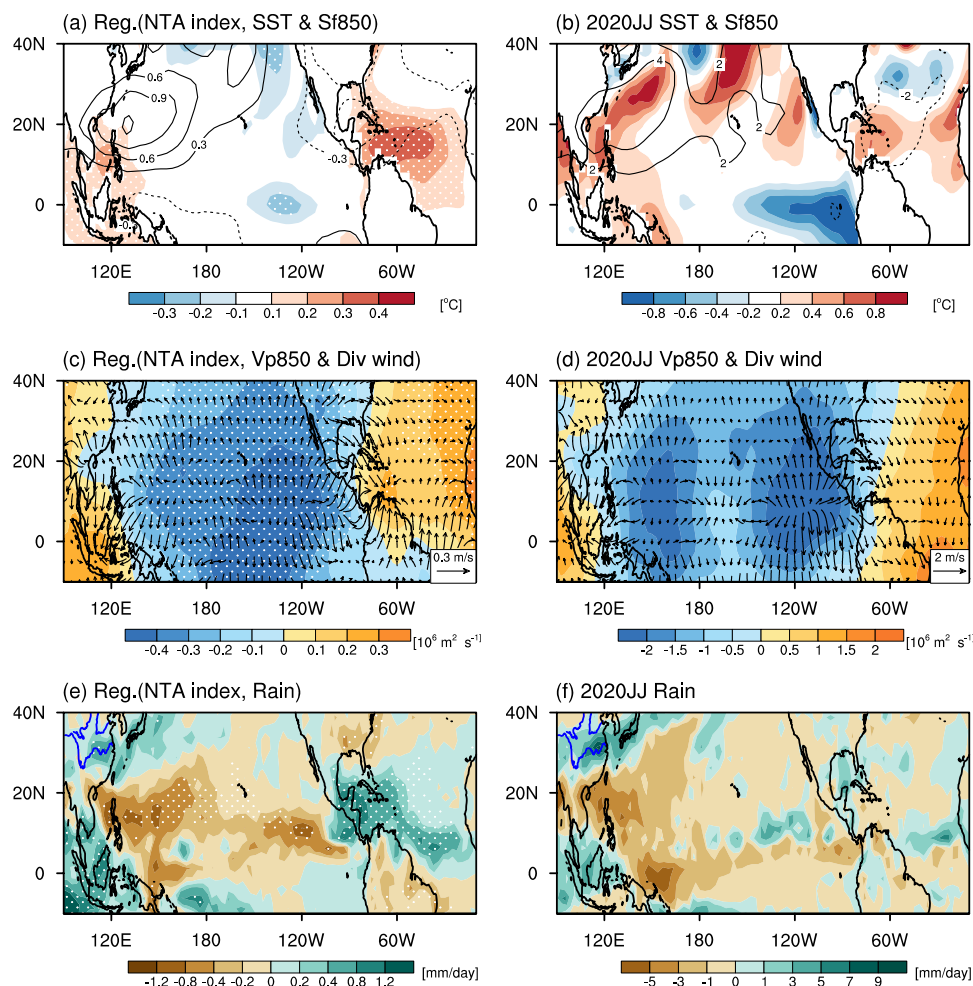
4.2 Role of the NTA SSTAs

The observed result shows that the WNPAC may also be associated with the NTA SSTAs in the JJ of 2020. Many previous studies have verified the contribution to the WNPAC from the tropical Atlantic (Ham et al. 2013; Hong et al. 2014; Chen et al. 2015, 2018). For example, Hong et al. (2014) implied that the warm NTA SST excites a zonally overturning circulation anomaly, with descent motion over the equatorial central Pacific and ascent motion over the tropical Atlantic and eastern Pacific. The anomalous descent motion over the equatorial central Pacific induces a low-level anticyclonic anomaly to the west and therefore enhances the WNPAC. To investigate the possible physical processes connecting the positive SSTAs over the NTA region and the anomalous WNPAC as well as rainfall anomalies over the YRV in JJ 2020, the regressed results with respect onto the NTA SSTAs index and the anomalies in JJ 2020 are calculated.

Figure 10a shows the regression pattern of SSTAs and lower tropospheric stream function onto the NTA SSTAs index. Significant positive SSTAs occupy over large regions of the NTA Ocean. To the northwest of NTA positive SSTAs, anomalous cyclonic circulation in the lower

tropospheric stream function field is observed. Negative SSTAs are seen over the central to eastern equatorial Pacific, which is induced by surface northeasterly wind anomalies on the western flank of the cyclonic circulation. This result is consistent with previous studies (Ham et al. 2013; KucharSKI et al. 2007) which implied that the warm NTA SSTAs could affect the SST in the equatorial central Pacific and lead to the development of the La Niña event by enhancing the speed of climatologic trend wind. Positive SSTAs over NTA region and anomalous cyclonic circulation in the lower tropospheric stream function field are observed in JJ 2020 (Fig. 10b). Negative SSTAs are mainly located over the eastern equatorial Pacific. As a response to the positive SSTAs, large anomalous convergence circulation is seen over NTA region (Fig. 10c), which results in enhanced convective activities and positive rainfall anomalies (Fig. 10e). The anomalous convergence circulation (Fig. 10d) and rainfall (Fig. 10f) in JJ 2020 located to the east compared to the regressed results. Anomalous diabatic heating associated with positive rainfall anomalies cause the anomalous cyclonic circulation (Fig. 10a, b) via a Gill-pattern Rossby wave response (Gill 1980). Anomalous divergence circulation is located over large areas of North Pacific in both the regressed field and in JJ 2020 (Fig. 10c, d). The upper-level convergence circulation anomalies are opposite to that in the lower-level field (figure is not shown), which indicates a zonal overturning vertical circulation between the North Atlantic and Pacific regions, consistent with findings in previous studies (Hong et al. 2014). Anomalous divergent circulation in the tropical Pacific result in anomalous descending motion and accordingly, negative rainfall anomaly occurred over the subtropical Pacific (Fig. 10e, f). The associated diabatic cooling anomalies induce an anticyclonic anomaly

Fig. 10 Regression of **a** SST anomaly (shadings; $^{\circ}\text{C}$) and 850 hPa stream function anomaly (contours; $10^6 \text{ m}^2 \text{ s}^{-1}$), **c** 850 hPa velocity potential anomaly (shading; $10^6 \text{ m}^2 \text{ s}^{-1}$) and the corresponding divergent wind anomaly (vectors; m s^{-1}), **e** rainfall anomaly (mm day^{-1}) with respect onto the normalized NTA SSTAs index averaged over JJ for the 1980–2020 period. **(b, d, f)** Same as **(a, c, e)**, but for the anomalies in JJ 2020. Dots in **(a, c, e)** denote where the regression coefficients exceed the 90% confidence level based on Student's *t* test



center in the WNP via the Gill response (Fig. 10a, b). Thus, it implies a teleconnection between the NTA SSTAs and the anomalous WNPAC. Finally, the anomalous southwesterly flow on the western edge of the WNPAC enhances moisture flux transport to the YRV region and results in positive anomalies there (Fig. 10e, f). Thus, positive SSTAs in the NTA region play an important role in the maintenance of the strong WNPAC and the extreme rainfall over YRV in JJ 2020 by inducing an atmospheric teleconnection.

5 Summary and discussion

This study investigated the extreme flood over the YRV in JJ 2020 and the possible factors using observational dataset and statistical analyses. The amount of rainfall over the YRV in JJ 2020, which was approximately 63% more than the climatology averaged during 1980–2020, resulted in a record-breaking flood in this region since 1980. It is suggested that the warm NIO condition seem to dominate the heavy rainfall in China in JJ 2020. The present study confirmed the contribution of the NIO warming and showed

two underlying processes by conducting statistical analysis. Besides, we found that the warm NTA SSTAs also contributed to the extreme flood event in YRV.

In JJ 2020, warm conditions in the NIO facilitated the enhanced YRV rainfall by strengthening the WNPAC and intensifying the moisture flux transportation to the YRV. Positive SSTAs in the NIO induced an eastward propagating Kelvin wave and suppressed convective activities over the WNP and enhanced the WNPAC. The associated easterly wind anomalies on the southern flank of the WNPAC weakened climatology westerlies wind and reduced surface evaporation, facilitating the maintenance of the warming condition over the NIO. Positive feedback between the WNPAC and the NIO warming intensified the magnitude and temporal persistence of the WNPAC. Alternately, positive SSTAs over the NIO impact the WNPAC by an anomalous reversed Walker circulation between the NIO and SCS-Philippine Sea regions. As a result, southwesterly wind anomalies on the western flank of the WNPAC transported abundant moisture flux from tropical oceans and increased summer rainfall over YRV in JJ 2020.

In addition to the role of positive SSTAs over the NIO, positive SSTAs over the NTA also contributed to the strong anomalous WNPAC and the above normal rainfall in YRV via an atmospheric teleconnection. The NTA warm SSTAs first caused a zonal overturning circulation between the NTA and tropical Pacific regions, with anomalous ascent motion over the NTA and anomalous descent motion over the central-eastern Pacific. The anomalous descent motion caused decreased rainfall in the tropical central-eastern Pacific, which led to the WNPAC via a Rossby wave response related to the anomalous diabatic heating. The results also show that the contribution from positive SSTAs in the NIO to the WNPAC and positive rainfall anomalies in the YRV is larger than that from positive SSTAs in the NTA region. Therefore, the anomalous WNPAC, which is generated and maintained by the effects of the warming SSTAs over the NIO and NTA regions, gave rise to the extreme flood event in the YRV in JJ 2020 by transporting unusually large number of water vapor fluxes from the tropical oceans.

A severe flood also occurred in YRV in 1998 summer. During 1997–98, a super El Niño event occurred in the equatorial eastern Pacific. Many studies have revealed the dominant influences of the 1997/98 El Niño on the extreme floods in YRV (Huang et al. 1998; Yuan et al. 2017; Chen et al. 2019). Warm conditions of the IO and SCS in summer 1998 were generated by the major El Niño through the IPOC mode (Xie et al. 2016). The Indian Ocean and SCS warming forced an anomalous anticyclone in the lower troposphere over the Indo-Northwest Pacific region and anomalous convergence of moisture flux in the mid and lower reaches of the YRV region (Yuan et al. 2017). Similar circulation anomalies and SSTA pattern in the tropical Indian Ocean happened for summer 2020. However, only a weak El Niño occurred in central Pacific in the preceding winter of 2020. It is suggested that the warm IO condition can be traced back to the super Indian Ocean Dipole (IOD) event in late 2019 (Takaya et al. 2020; Zhou et al. 2021). The record-breaking IOD sustains the IO warming through the summer 2020 by oceanic dynamics processes and monsoon modulation. Therefore, it indicated that the major Yangtze River flood happened in summer 1998 is a typical case of the warm IO and SCS that followed a super El Niño event in previous winter, whereas the extreme flood in summer 2020 is not anticipated from El Niño conditions but coupled ocean–atmosphere processes in the Indian Ocean. In addition, positive SST anomalies in NTA also contribute to the extreme flood in YRV in summer 2020 through an anomalous zonal vertical circulation. In summer 1998, previous studies showed that a strong negative phase of North Atlantic triple mode plays an important role in the extreme flood along the YRV by stimulating a stronger than normal Ural high through a zonal teleconnection wave pattern across the Eurasian continent (Yuan et al. 2017).

The present study suggests that warming SSTAs over the NIO and NTA regions are two important factors influencing the extreme flood event over the YRV in JJ 2020. However, the reconstructed rainfall anomaly over the YRV in JJ 2020 using the NIO and NTA SSTAs indices (Fig. 7) is less than observed rainfall anomaly (Fig. 3a). It seems that other factors, such as the middle and high latitude systems (Li et al. 2017; Li and Lu 2017), the Arctic sea ice extent (Wu et al. 2009; Zhao et al. 2004) as well as the global warming (Li et al. 2018; Ma et al. 2020; Zhu et al. 2016) may also play a role in modulating the rainfall anomaly in the YRV in JJ 2020. The co-effects of the tropical and extratropical factors on the extreme flood event over the YRV in JJ 2020 require further investigation. This study attempts to investigate ocean roles by conducting the statistical analysis using historical data. The statistical analysis does not give the statistical confidence level for a particular event. This weakness may be partially overcome by verifying the sequence of processes and supporting results with modeling experiments in future study. In addition, Takaya et al. (2020) pointed that the warming SST over the NIO was related to the super positive Indian Ocean Dipole (IOD) in 2019. The mechanism for the formation of the positive SSTAs over NTA is unclear and remains an interesting issue for future study.

Author contribution All the authors contributed to conceptualize and design the study. Data were gathered by Xiaoxue Yin; an initial draft of the paper was prepared by Xiaoxue Yin; the article was repeatedly revised to generate the final version by Lian-Tong Zhou, Kui Liu, Yongqiu Han, and Zhaoyang Du.

Funding This study was funded by the National Key Research and Development Program of China (2016YFA0600603) and the National Natural Science Foundation of China (grant no. 42105063).

Data availability Data that support the findings of this study are openly available online. The CMAP data are freely available at <https://psl.noaa.gov/data/gridded/data.cmap.html>. The NECP-DOE reanalysis data are freely available at <https://psl.noaa.gov/data/gridded/data.ncep.reanalysis2.html>. The ERSST.v5b data are freely available at <https://psl.noaa.gov/data/gridded/data.noaa.ersst.v5.html>.

Code availability The codes used for the processing of data can be provided on request to the corresponding author.

Declarations

Ethics approval Not applicable.

Consent to participate Not applicable.

Consent for publication All the authors consented to publish the paper.

Conflict of interest The authors declare no competing interests.

References

- Annamalai H, Liu P, Xie SP (2005) Southwest Indian Ocean SST variability: its local effect and remote influence on Asian monsoons. *J Climate* 18:4150–4167. <https://doi.org/10.1175/jcli3533.1>
- Ashok K, Behera SK, Rao SA, Weng HY, Yamagata T (2007) El Niño Modoki and its possible teleconnection. *J Geophys Res Oceans* 112. <https://doi.org/10.1029/2006jc003798>
- Chang CP, Zhang YS, Li T (2000) Interannual and interdecadal variations of the East Asian summer monsoon and tropical Pacific SSTs. Part I: Roles of the subtropical ridge. *J Climate* 13:4310–4325. [https://doi.org/10.1175/1520-0442\(2000\)013%3c4310:iaivot%3e2.0.Co;2](https://doi.org/10.1175/1520-0442(2000)013%3c4310:iaivot%3e2.0.Co;2)
- Chen Y, Zhai P (2013) Persistent extreme precipitation events in China during 1951–2010. *Climate Res* 57:143–155. <https://doi.org/10.3354/cr01171>
- Chen Y, Zhai P (2015) Synoptic-scale precursors of the East Asia/Pacific teleconnection pattern responsible for persistent extreme precipitation in the Yangtze River Valley. *Quart J Roy Meteor Soc* 141:1389–1403. <https://doi.org/10.1002/qj.2448>
- Chen W, Lee J-Y, Lu R, Dong B, Ha K-J (2015) Intensified impact of tropical Atlantic SST on the western North Pacific summer climate under a weakened Atlantic thermohaline circulation. *Climate Dyn* 45:2033–2046. <https://doi.org/10.1007/s00382-014-2454-4>
- Chen JP, Wang X, Zhou W, Wang CZ, Xie Q, Li G, Chen S (2018) Unusual rainfall in southern China in decaying August during extreme El Niño 2015/16: role of the western Indian Ocean and north tropical Atlantic SST. *J Climate* 31:7019–7034. <https://doi.org/10.1175/jcli-d-17-0827.1>
- Chen D, Gao Y, Wang H (2019) Why was the August rainfall pattern in the East Asia-Pacific Ocean region in 2016 different from that in 1998 under a similar preceding El Niño background? *J Climate* 32:5785–5797. <https://doi.org/10.1175/JCLI-D-18-0589.1>
- Chen J, Yu J-Y, Wang X, Lian T (2020) Different influences of south-eastern Indian Ocean and western Indian Ocean SST anomalies on Eastern China rainfall during the decaying summer of the 2015/16 extreme El Niño. *J Climate* 33:5427–5443. <https://doi.org/10.1175/JCLI-D-19-0777.1>
- Ding Y (1992) Summer monsoon rainfalls in China. *J Meteor Soc Japan* 70:373–396. https://doi.org/10.2151/jmsj1965.70.1B_373
- Ding Y, Liang P, Liu Y, Zhang Y (2020) Multiscale variability of Meiyu and its prediction: a new review. *J Geophys Res Atmos* 125. <https://doi.org/10.1029/2019jd031496>
- Ding Y, Liu Y, Hu Z-Z (2021) The record-breaking Meiyu in 2020 and associated atmospheric circulation and tropical SST anomalies. *Adv Atmos Sci* 1–14. <https://doi.org/10.1007/s00376-021-0361-2>
- Du Y, Xie S-P, Huang G, Hu K (2009) Role of air-sea interaction in the long persistence of El Niño-induced north Indian Ocean warming. *J Climate* 22:2023–2038. <https://doi.org/10.1175/2008jcli2590.1>
- Emanuel KA, Neelin JD, Bretherton CS (1997) On large-scale circulations in convecting atmospheres - reply. *Quart J Roy Meteor Soc* 123:1779–1782. <https://doi.org/10.1002/qj.49712354217>
- Gao Y, Wang H, Chen D (2018) Precipitation anomalies in the Pan-Asian monsoon region during El Niño decaying summer 2016. *Int J Climatol* 38:3618–3632. <https://doi.org/10.1002/joc.5522>
- Gill AE (1980) Some simple solutions for heat-induced tropical circulation. *Quart J Roy Meteor Soc* 106:447–462. <https://doi.org/10.1256/smsqj.44904>
- Gong DY, Ho CH (2002) Shift in the summer rainfall over the Yangtze River valley in the late 1970s. *Geophys Res Lett* 29. <https://doi.org/10.1029/2001gl014523>
- Gu W, Li C, Wang X, Zhou W, Li W (2009) Linkage between Meiyu precipitation and North Atlantic SST on the decadal time-scale. *Adv Atmos Sci* 26:101–108. <https://doi.org/10.1007/s00376-009-0101-5>
- Guo YF, Zhao Y, Wang J (2002) Numerical simulation of the relationships between the 1998 Yangtze River valley floods and SST anomalies. *Adv Atmos Sci* 19:391–404
- Ham Y-G, Kug J-S, Park J-Y, Jin F-F (2013) Sea surface temperature in the north tropical Atlantic as a trigger for El Niño/Southern Oscillation events. *Nat Geosci* 6:112–116. <https://doi.org/10.1038/ngeo1686>
- He Z, Wu R (2014) Indo-Pacific remote forcing in summer rainfall variability over the South China Sea. *Climate Dyn* 42:2323–2337. <https://doi.org/10.1007/s00382-014-2123-7>
- Holton JR (2004) *An Introduction to Dynamic Meteorology*. Academic Press
- Hong C-C, Chang T-C, Hsu H-H (2014) Enhanced relationship between the tropical Atlantic SST and the summertime western North Pacific subtropical high after the early 1980s. *J Geophys Res Atmos* 119:3715–3722. <https://doi.org/10.1002/2013jd021394>
- Huang RH, Li WJ (1988) Influence of heat source anomaly over the western tropical Pacific on the subtropical high over East Asia and its physical mechanism. *Chinese J Atmos Sci* 12(s1):107–116 (in Chinese)
- Huang RH, Sun FY (1992) Impacts of the tropical western Pacific on the East-Asian summer monsoon. *J Meteor Soc Japan* 70:243–256. https://doi.org/10.2151/jmsj1965.70.1B_243
- Huang RH, Wu YF (1989) The influence of ENSO on the summer climate change in China and its mechanism. *Adv Atmos Sci* 6:21–21
- Huang R, Zhou L (2002) Research on the characteristics, formation mechanism and prediction of severe climatic disasters in China. *J Nat Disast (in Chinese)* 11:1–9
- Huang R, Xu Y, Wang P, Zhou L (1998) The features of the catastrophic flood over the Changjiang River Basin during the summer of 1998 and cause exploration. *Climatic Environ Res* 3:300–313 (in Chinese)
- Huang B et al (2017) Extended reconstructed sea surface temperature, version 5 (ERSSTv5): Upgrades, validations, and inter-comparisons. *J Climate* 30:8179–8205. <https://doi.org/10.1175/jcli-d-16-0836.1>
- Huangfu J, Huang R, Chen W, Feng T (2018) Causes of the active typhoon season in 2016 following a strong El Niño with a comparison to 1998. *Int J Climatol* 38:e1107–e1118. <https://doi.org/10.1002/joc.5437>
- Jiang T, Kundzewicz ZW, Su B (2008) Changes in monthly precipitation and flood hazard in the Yangtze River Basin, China. *Int J Climatol* 28:1471–1481. <https://doi.org/10.1002/joc.1635>
- Kanamitsu M, Ebisuzaki W, Woollen J, Yang SK, Hnilo JJ, Fiorino M, Potter GL (2002) NCEP-DOE AMIP-II reanalysis (R-2). *Bull Amer Meteor Soc* 83:1631–1643. [https://doi.org/10.1175/bams-83-11-1631\(2002\)083%3c1631:Nar%3e2.3.Co;2](https://doi.org/10.1175/bams-83-11-1631(2002)083%3c1631:Nar%3e2.3.Co;2)
- Klein SA, Soden BJ, Lau NC (1999) Remote sea surface temperature variations during ENSO: evidence for a tropical atmospheric bridge. *J Climate* 12:917–932. [https://doi.org/10.1175/1520-0442\(1999\)012%3c0917:Rsstvd%3e2.0.Co;2](https://doi.org/10.1175/1520-0442(1999)012%3c0917:Rsstvd%3e2.0.Co;2)
- Kosaka Y, Xie S-P, Lau N-C, Vecchi GA (2013) Origin of seasonal predictability for summer climate over the Northwestern Pacific. *Proc Natl Acad Sci USA* 110:7574–7579. <https://doi.org/10.1073/pnas.1215582110>
- Kucharski F, Bracco A, Yoo JH, Molteni F (2007) Low-frequency variability of the Indian monsoon-ENSO relationship and the tropical atlantic: the “Weakening” of the 1980s and 1990s. *J Climate* 20:4255–4266. <https://doi.org/10.1175/jcli4254.1>
- Lau KM, Weng HY (2001) Coherent modes of global SST and summer rainfall over China: an assessment of the regional impacts of the 1997–98 El Niño. *J Climate* 14:1294–1308. [https://doi.org/10.1175/1520-0442\(2001\)014%3c1294:Cmogs%3e2.0.Co;2](https://doi.org/10.1175/1520-0442(2001)014%3c1294:Cmogs%3e2.0.Co;2)

- Li XY, Lu RY (2017) Extratropical factors affecting the variability in summer precipitation over the Yangtze River basin, China. *J Climate* 30:8357–8374. <https://doi.org/10.1175/jcli-d-16-0282.1>
- Li S, Lu J, Huang G, Hu K (2008) Tropical Indian Ocean basin warming and East Asian summer monsoon: a multiple AGCM study. *J Climate* 21:6080–6088. <https://doi.org/10.1175/2008jcli2433.1>
- Li CF, Chen W, Hong XW, Lu RY (2017) Why was the strengthening of rainfall in summer over the Yangtze River valley in 2016 less pronounced than that in 1998 under similar preceding El Niño events?—Role of midlatitude circulation in August. *Adv Atmos Sci* 34:1290–1300. <https://doi.org/10.1007/s00376-017-7003-8>
- Li CX et al (2018) Attribution of extreme precipitation in the lower reaches of the Yangtze River during May 2016. *Environ Res Lett* 13. <https://doi.org/10.1088/1748-9326/aa9691>
- Lindzen RS, Nigam S (1987) On the role of sea surface temperature gradients in forcing low-level winds and convergence in the tropics. *J Atmos Sci* 44:2418–2436. [https://doi.org/10.1175/1520-0469\(1987\)044%3c2418:Otross%3e2.0.Co;2](https://doi.org/10.1175/1520-0469(1987)044%3c2418:Otross%3e2.0.Co;2)
- Liu BQ, Yan YH, Zhu CW, Ma SM, Li JY (2020) Record-breaking Meiyu rainfall around the Yangtze River in 2020 regulated by the subseasonal phase transition of the North Atlantic oscillation. *Geophys Res Lett* 47:ARTN e2020GL090342 <https://doi.org/10.1029/2020GL090342>
- Luo Y, Wang H, Zhang R, Qian W, Luo Z (2013) Comparison of rainfall characteristics and convective properties of monsoon precipitation systems over South China and the Yangtze and Huai River basin. *J Climate* 26:110–132. <https://doi.org/10.1175/jcli-d-12-00100.1>
- Ma S, Zhu C, Liu J (2020) Combined impacts of warm central equatorial Pacific sea surface temperatures and anthropogenic warming on the 2019 severe drought in East China. *Adv Atmos Sci* 37:1149–1163. <https://doi.org/10.1007/s00376-020-0077-8>
- Ninomiya K, Shibagaki Y (2007) Multi-scale features of the Meiyu-Baiu front and associated precipitation systems. *J Meteor Soc Japan* 85B:103–122. <https://doi.org/10.2151/jmsj.85B.103>
- Nitta T (1987) Convective activities in the tropical western Pacific and their impact on the North Hemisphere summer circulation. *J Meteor Soc Japan* 65:373–390. https://doi.org/10.2151/jmsj1965.65.3_373
- Ohba M, Kadokura S, Yoshida Y, Nohara D, Toyoda Y (2015) Anomalous weather patterns in relation to heavy precipitation events in Japan during the Baiu season. *J Hydrometeorol* 16:688–701. <https://doi.org/10.1175/jhm-d-14-0124.1>
- Qiao S et al (2021) The longest 2020 Meiyu season over the past 60 years: subseasonal perspective and Its predictions. *Geophys Res Lett* 48:e2021GL093596. <https://doi.org/10.1029/2021GL093596>
- Rong X, Zhang R, Li T (2010) Impacts of Atlantic sea surface temperature anomalies on Indo-East Asian summer monsoon-ENSO relationship. *Chinese Sci Bull* 55:2458–2468. <https://doi.org/10.1007/s11434-010-3098-3>
- Takaya Y, Ishikawa I, Kobayashi C, Endo H, Ose T (2020) Enhanced Meiyu-Baiu rainfall in early summer 2020: Aftermath of the 2019 super IOD event. *Geophys Res Lett* 47. <https://doi.org/10.1029/2020gl090671>
- Wakabayashi S, Kawamura R (2004) Extraction of major teleconnection patterns possibly associated with the anomalous summer climate in Japan. *J Meteor Soc Japan* 82:1577–1588. <https://doi.org/10.2151/jmsj.82.1577>
- Wang B, Zhang Q (2002) Pacific-east Asian teleconnection. Part II: how the Philippine Sea anomalous anticyclone is established during El Niño development. *J Climate* 15:3252–3265. [https://doi.org/10.1175/1520-0442\(2002\)015%3c3252:Peatpi%3e2.0.Co;2](https://doi.org/10.1175/1520-0442(2002)015%3c3252:Peatpi%3e2.0.Co;2)
- Wang B, Wu RG, Lau KM (2001) Interannual variability of the Asian summer monsoon: contrasts between the Indian and the western North Pacific-east Asian monsoons. *J Climate* 14:4073–4090. [https://doi.org/10.1175/1520-0442\(2001\)014%3c4073:Ivotas%3e2.0.Co;2](https://doi.org/10.1175/1520-0442(2001)014%3c4073:Ivotas%3e2.0.Co;2)
- Wu RG, Hu ZZ, Kirtman BP (2003) Evolution of ENSO-related rainfall anomalies in East Asia. *J Climate* 16:3742–3758. [https://doi.org/10.1175/1520-0442\(2003\)016%3c3742:Eoerai%3e2.0.Co;2](https://doi.org/10.1175/1520-0442(2003)016%3c3742:Eoerai%3e2.0.Co;2)
- Wu B, Zhang R, Wang B (2009) On the association between spring Arctic sea ice concentration and Chinese summer rainfall: a further study. *Adv Atmos Sci* 26:666–678. <https://doi.org/10.1007/s00376-009-9009-3>
- Xie PP, Arkin PA (1997) Global precipitation: a 17-year monthly analysis based on gauge observations, satellite estimates, and numerical model outputs. *Bull Amer Meteor Soc* 78:2539–2558. [https://doi.org/10.1175/1520-0477\(1997\)078%3c2539:Gpayma%3e2.0.Co;2](https://doi.org/10.1175/1520-0477(1997)078%3c2539:Gpayma%3e2.0.Co;2)
- Xie S-P, Hu K, Hafner J, Tokinaga H, Du Y, Huang G, Sampe T (2009) Indian Ocean capacitor effect on Indo-Western Pacific climate during the summer following El Niño. *J Climate* 22:730–747. <https://doi.org/10.1175/2008jcli2544.1>
- Xie S-P, Kosaka Y, Du Y, Hu K, Chowdary JS, Huang G (2016) Indo-western Pacific ocean capacitor and coherent climate anomalies in post-ENSO summer: a review. *Adv Atmos Sci* 33:411–432. <https://doi.org/10.1007/s00376-015-5192-6>
- Yang J, Liu Q, Xie S-P, Liu Z, Wu L (2007) Impact of the Indian Ocean SST basin mode on the Asian summer monsoon. *Geophys Res Lett* 34. <https://doi.org/10.1029/2006GL028571>
- Yin X, Zhou L-T (2019) An interdecadal change in the influence of the Central Pacific ENSO on the subsequent north tropical Atlantic spring SST variability around the mid-1980s. *Climate Dyn* 53:879–893. <https://doi.org/10.1007/s00382-019-04618-2>
- Yin X, Zhou L-T (2020) Strengthened relationships of northwest China wintertime precipitation with ENSO and midlatitude north Atlantic SST since the mid-1990s. *J Climate* 33:3967–3988. <https://doi.org/10.1175/jcli-d-19-0454.1>
- Yuan Y, Gao H, Li W, Liu Y, Chen L, Zhou B, Ding Y (2017) The 2016 summer floods in China and associated physical mechanisms: a comparison with 1998. *J Meteor Res* 31:261–277. <https://doi.org/10.1007/s13351-017-6192-5>
- Zhang RH, Sumi A, Kimoto M (1999) A diagnostic study of the impact of El Niño on the precipitation in China. *Adv Atmos Sci* 16:229–241. <https://doi.org/10.1007/bf02973084>
- Zhang Y, Zhou W, Leung MYT (2019) Phase relationship between summer and winter monsoons over the South China Sea: Indian Ocean and ENSO forcing. *Climate Dyn* 52:5229–5248. <https://doi.org/10.1007/s00382-018-4440-8>
- Zhao P, Zhang XD, Zhou XJ, Ikeda M, Yin YH (2004) The sea ice extent anomaly in the North Pacific and its impact on the East Asian summer monsoon rainfall. *J Climate* 17:3434–3447. [https://doi.org/10.1175/1520-0442\(2004\)017%3c3434:Tsieai%3e2.0.Co;2](https://doi.org/10.1175/1520-0442(2004)017%3c3434:Tsieai%3e2.0.Co;2)
- Zheng J, Wang C (2021) Influences of three oceans on record-breaking rainfall over the Yangtze River Valley in June 2020. *Sci China-Earth Sci*. <https://doi.org/10.1007/s11430-020-9758-9>
- Zhou W, Chan JCL (2007) ENSO and the South China Sea summer monsoon onset. *Int J Climatol* 27:157–167. <https://doi.org/10.1002/joc.1380>
- Zhou Y, Gao S, Shen SSP (2004) A diagnostic study of formation and structures of the Meiyu front system over East Asia. *J Meteor Soc Japan* 82:1565–1576. <https://doi.org/10.2151/jmsj.82.1565>
- Zhou Z-Q, Xie S-P, Zhang R (2021) Historic Yangtze flooding of 2020 tied to extreme Indian Ocean conditions. *Proc Natl Acad Sci* 118:e2022255118. <https://doi.org/10.1073/pnas.2022551118>

- Zhou TJ, Yu RC (2005) Atmospheric water vapor transport associated with typical anomalous summer rainfall patterns in China. *J Geophys Res Atmos* 110. <https://doi.org/10.1029/2004jd005413>
- Zhu J, Huang D, Yang T (2016) Changes of Meiyu system in the future under A1B scenario simulated by MIROC_Hires model. *Theor Appl Climatol* 123:461–471. <https://doi.org/10.1007/s00704-015-1371-8>
- Zong YQ, Chen XQ (2000) The 1998 flood on the Yangtze, China. *Natl Hazards* 22:165–184. <https://doi.org/10.1023/a:1008119805106>

Publisher's note Springer Nature remains neutral with regard to jurisdictional claims in published maps and institutional affiliations.

Springer Nature or its licensor holds exclusive rights to this article under a publishing agreement with the author(s) or other rightsholder(s); author self-archiving of the accepted manuscript version of this article is solely governed by the terms of such publishing agreement and applicable law.